water

Article

A Grid-Based Long Short-Term Memory Framework for Runoff Projection and Uncertainty in the Yellow River Source Area Under CMIP6 Climate Change

Haibo Chu [1,*], Yulin Jiang [1] and Zhuoqi Wang [2]

[1] College of Architecture and Civil Engineering, Beijing University of Technology, Beijing 100124, China; 18315010507@163.com
[2] Beijing Goldenwater Information Technology Co., Ltd., Beijing 100124, China; wzq15830908316@163.com
* Correspondence: chuhaibo@bjut.edu.cn

Abstract: Long-term runoff projection and uncertainty estimates can provide both the changing trends and confidence intervals of water resources, provide basic information for decision makers, and reduce risks for water resource management. In this paper, a grid-based runoff projection and uncertainty framework was proposed through input selection and long short-term memory (LSTM) modelling coupled with uncertainty analysis. We simultaneously considered dynamic variables and static variables in the candidate input combinations. Different input combinations were compared. We employed LSTM to develop a relationship between monthly runoff and the selected variables and demonstrated the improvement in forecast accuracy through comparison with the MLR, RBFNN, and RNN models. The LSTM model achieved the highest mean Kling–Gupta Efficiency (KGE) score of 0.80, representing respective improvements of 45.45%, 33.33%, and 2.56% over the other three models. The uncertainty sources originating from the parameters of the LSTM models were considered, and the Monte Carlo approach was used to provide uncertainty estimates. The framework was applied to the Yellow River Source Area (YRSR) at the 0.25° grid scale to better show the temporal and spatial features. The results showed that extra information about static variables can improve the accuracy of runoff projections. Annual runoff tended to increase, with projection ranges of 148.44–296.16 mm under the 95% confidence level, under various climate scenarios.

Keywords: runoff projection; uncertainty; grid; LSTM; CMIP6

Academic Editor: Athanasios Loukas

Received: 29 November 2024
Revised: 10 February 2025
Accepted: 26 February 2025
Published: 4 March 2025

Citation: Chu, H.; Jiang, Y.; Wang, Z. A Grid-Based Long Short-Term Memory Framework for Runoff Projection and Uncertainty in the Yellow River Source Area Under CMIP6 Climate Change. *Water* **2025**, *17*, 750. https://doi.org/10.3390/w17050750

1. Introduction

For long-term water resource planning in large basins, long-term runoff projection can offer trend information. Uncertainty analysis can lower the risk associated with water resource management by providing extra information regarding confidence ranges or probabilistic predicted runoff [1,2]. An integrated model or a chain-based framework has shown promise for accurate, reliable, and stable runoff projection, which involves large uncertainties due to the combination of several climatic and hydrological models, as well as machine learning models [3,4].

Long short-term memory (LSTM), which is well known for its machine learning approach, has been extensively utilized for runoff projection in various applications and has great potential for understanding unknown hydrological mechanism processes. Sahoo et al. (2019) evaluated the effectiveness of LSTM in low-streamflow forecasting relative to recurrent neural networks (RNNs) [5]. Xiang et al. (2020) constructed an LSTM model for runoff prediction in Iowa with observed and forecasted rainfall, observed runoff, and evapotranspiration [6]. Hunt et al. (2022) used observed streamflow and meteorological factors to train an LSTM model that predicted streamflow at ten locations in different climatic zones of the US [7]. Khoshkalam et al. (2023) utilized LSTM with an input processing method to enhance the precision of streamflow forecasting [8]. Their findings showed that the LSTM model is capable of efficiently retrieving knowledge from large data information and hydrology systems with different input data. However, many details about parameter determination, performance comparison, and uncertainty in the application of LSTM modelling for runoff projection still exist and need to be further discussed.

Uncertainty analysis is another component of a data-driven model framework in which process uncertainty originates from emission scenarios, climate models, hydrological modelling, probability distributions, etc. [9,10]. Zhang et al. (2021) estimated how the high streamflow would be affected by climate change in the YRSR with a chain-based numerical simulation modelling system and quantified the uncertainty contribution of all the chain elements [11]. The structural design and parameter settings of hydrological models or data-driven models are the dominant sources of uncertainty in the framework. Therefore, providing different confidence intervals of runoff projections under uncertainty from the structure and parameters is highly important. MC is a traditional technique that has been effectively used in many hydrology fields [12,13].

Physical–mechanical models, including VIC and SWAT, coupled with future climate scenarios from CMIP5 or CMIP6, have been used for runoff projections of the Yellow River. Liu et al. (2011) used SWAT and CMIP5 data for runoff projection to forecast flows in both present and future climatic scenarios. Ji et al. (2023) employed a surface–subsurface process land surface model and CMIP6 bias-corrected data to perform future projections [14]. Zhou et al. (2023) coupled the VIC model with CMIP6 mid-high warming scenarios for runoff projections of major Chinese basins, and it indicated a discernible upward trend in runoff within the YRSR under the two high-temperature scenarios [15]. However, most previous studies have focused on runoff projection and uncertainty only at the station scale via hydrological models, and revealing temporal variations is still difficult. Therefore, a framework based on the LSTM model for runoff projection at the grid scale and uncertainty estimates should be studied further to allow for high-resolution spatial predictions.

In this paper, a grid-based LSTM runoff projection and uncertainty framework was proposed through input selection, LSTM modelling, and uncertainty analysis. We simultaneously considered dynamic variables and static variables in the candidate inputs. Different input combinations were compared. We employed LSTM to develop a relationship between monthly runoff and the selected variables and analyzed it with the other models. The uncertainty sources originating from the parameters of the LSTM models were considered, and the Monte Carlo approach was used to provide uncertainty estimates.

2. Materials and Methods

A grid-based LSTM framework for runoff projection and uncertainty encompasses input selection, LSTM modelling, and uncertainty analysis. The framework's process is illustrated in Figure 1. The outputs of the LSTM model are the monthly runoff values for each grid cell. The inputs to the LSTM model include precipitation, temperature, and antecedent runoff, along with their corresponding lagged times, as well as static variables such as the Digital Elevation Model (DEM) and the Normalized Difference Vegetation Index (NDVI), which are determined through input selection.

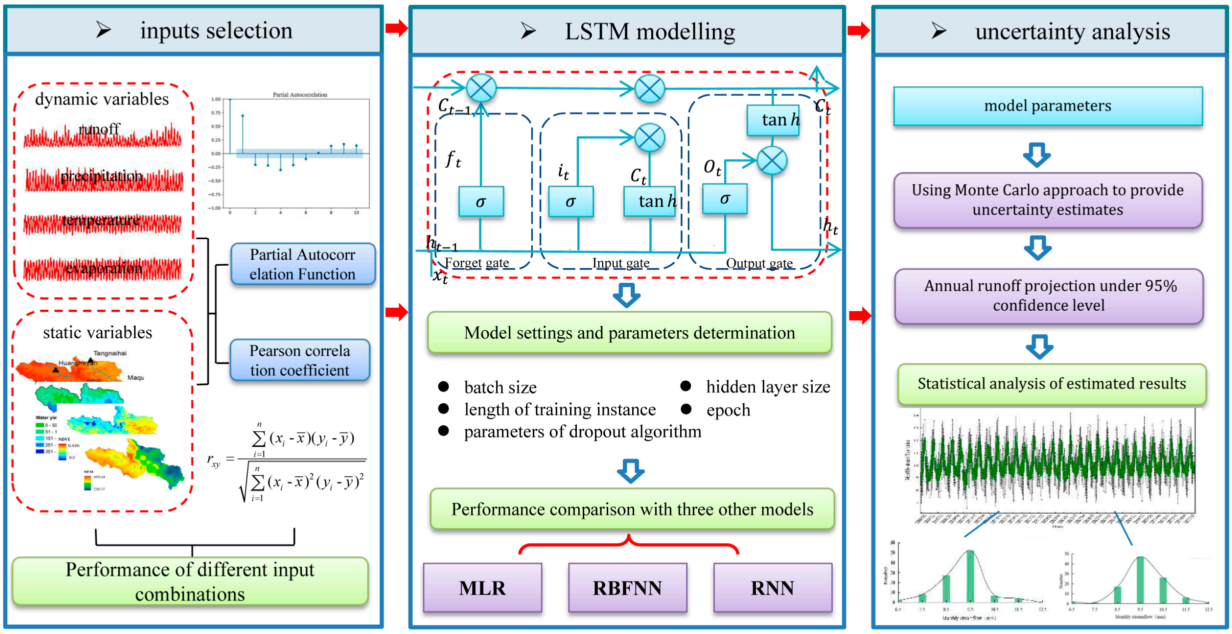

Figure 1. Structural diagram for the LSTM-based framework, including input selection, LSTM modelling, and uncertainty analysis.

2.1. Select Input

The runoff generation process is influenced by various factors within the complex hydrological system, and runoff projections are made by analyzing the relationships between runoff and other variables in this system. The variables associated with runoff serve as potential input variables. However, some variables that exhibit weak correlations with runoff or lack real-time variability are often excluded from consideration [16]. It is not necessary to include all variables in the hydrological system to establish the relationship between variables and runoff. Research has shown that models concentrating on the relationships between key variables and runoff can achieve higher prediction accuracies compared to models that incorporate all available variables [17].

2.2. LSTM

The long short-term memory (LSTM) model was developed to address the vanishing and exploding gradient problems commonly encountered in the computational processes of recurrent neural networks (RNNs). It establishes a robust connection between historical hydro-meteorological data and current hydrological data [18,19]. Typically, a three-layer LSTM network is employed, consisting of input, hidden, and output layers. The primary parameters discussed in this paper include batch size, hidden layers, epochs, dropout methods, and the duration of training instances. Batch size determines the number of training examples provided to the model for loss function calculation before updating the weight matrices [20]. The hidden layers represent the number of layers between the input and output, indicating a higher level of network complexity. An epoch refers to a complete forward pass through all training examples. The duration of training instances defines the length of the time series for each training sample. Dropout is a regularization technique specifically designed for neural networks, which randomly removes network nodes and their connections [21]. The extent of regularization is controlled by a parameter known as the dropout rate, which indicates the percentage of units excluded during training. In this framework, the parameters and structure of long short-term memory (LSTM) models were considered. The LSTM model's hyperparameters, including the dropout rate, number of epochs, and hidden units, were optimized using a grid search strategy to assure the best model performance, and the Monte Carlo approach was employed to provide uncertainty estimates. The Monte Carlo simulations were run with 1000 iterations to ensure robust uncertainty estimates [22,23]. The choice of 1000 iterations was based on preliminary convergence tests, which indicated that this number provided stable estimates of metrics.

2.3. Model Evaluation Criteria

In the current investigation, the effectiveness of various models was comprehensively evaluated using the coefficient of determination (R^2), Nash–Sutcliffe Efficiency (NSE), root-mean-square error (RMSE), and Kling–Gupta Efficiency coefficient (KGE). The formulas for these model evaluation criteria are outlined below:

$$R^2 = \left(\frac{\sum_{i=1}^{n} (q_i - \overline{q})(Q_i - \overline{Q})}{\sqrt{\sum_{i=1}^{n} (q_i - \overline{q})^2 \sum_{i=1}^{n} (Q_i - \overline{Q})^2}} \right)^2 \tag{1}$$

$$RMSE = \sqrt{\frac{1}{n} \sum_{i=1}^{n} (Q_i - q_i)^2} \tag{2}$$

$$NSE = 1 - \frac{\sum_{i=1}^{n} (Q_i - q_i)^2}{\sum_{i=1}^{n} (q_i - \overline{q}_i)^2} \tag{3}$$

KGE is a metric in assessing the precision of LSTM models, and it is calculated at each grid, which is characterized as

$$KGE = 1 - \sqrt{(r-1)^2 + (v-1)^2 + (w-1)^2} \tag{4}$$

where r is defined as Pearson's correlation coefficient, v is defined as the ratio between the mean predicted and observed runoff (μ_{sim}/μ_{obs}), and w is characterized as the ratio of the predicted runoff's standard deviation to that of the observed runoff ($\sigma_{sim}/\sigma_{obs}$). The effectiveness of KGE stems from the inclusion of correlation, variability, and bias indicators, which enables a thorough evaluation of whether the model accurately replicates the observed hydrological behaviour or not [7].

3. Study Area and Data

3.1. Study Area

The Yellow River Source Area (YRSR) is located in Qinghai Province (95.84° E–103.47° E, 32.20° N–35.80° N) and the northeastern region of the Qinghai–Tibet Plateau, as illustrated in Figure 2. This source region encompasses an area of 124,000 km^2 above the Tangnaihai station, accounting for 15.7% of the entire basin. The length of the river within this region is approximately 1553 km. The elevation of the area ranges from 3480 to 4680 m [24,25]. Nearly 80% of the region is covered by grassland, while lakes and swamps occupy roughly 2000 km^2. The YRSR is classified as a semi-humid region on the Tibetan Plateau, with temperatures fluctuating between −4 °C and 2 °C [26]. The area receives an average annual precipitation of 534 mm, with a significant portion (75–90%) occurring during the rainy season, which lasts from June to September. A notable decline in precipitation is observed when moving from the southeast to the northwest; specifically, the southeastern region receives approximately 800 mm, while the northwestern region receives about 300 mm.

The average annual runoff is estimated to be 19.8×10^9 m^3, accounting for more than 42% of the total water resources within the Yellow River basin.

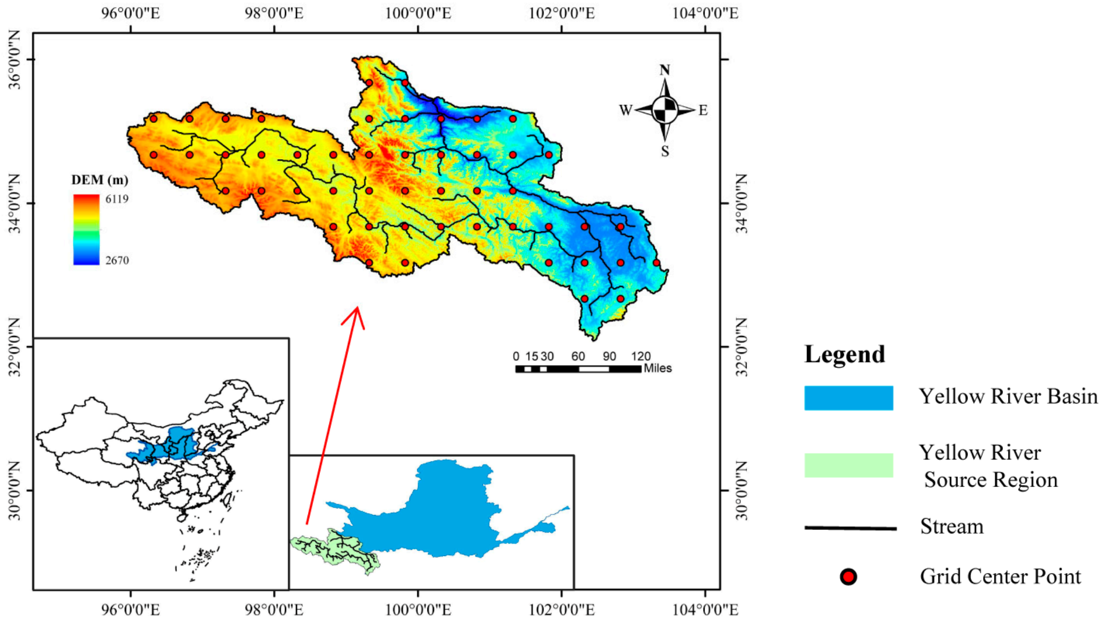

Figure 2. Location of the research area.

3.2. Datasets

The hydrological data are derived from the Chinese Natural Runoff Grid Dataset (CNRD v1.0), which encompasses a monthly runoff time series from 1961 to 2015 at a resolution of 0.25° × 0.25° [27]. The meteorological data, sourced from the ISIMIP, include precipitation and average temperature, with a grid resolution of 0.5° × 0.5°. Future runoff forecasts utilize the latest version of the NEX-GDDP-CMIP6 dataset. This dataset features globally downscaled climatic scenarios generated from General Circulation Model (GCM) operations conducted under the CMIP6 framework, covering all four categories of greenhouse gas emission scenarios identified as Shared Socioeconomic Pathways (SSPs) [28]. The climate model dataset from NASA, specifically NEX-GDDP-CMIP6, provides simulations for eight variables across five emission scenarios (historical, SSP126, SSP245, SSP370, and SSP585) using 35 global climate models. In this study, the Canadian Earth System Model (CanESM5) is employed to analyze meteorological data from the four Shared Socioeconomic Pathways [29,30].

4. Discussion

4.1. Input Selection

Eleven candidate input variables, including precipitation, air pressure, sunshine duration, temperature, and evaporation, were considered. The correlations between these input variables and runoff were quantitatively assessed using Pearson correlation analysis, and a heatmap illustrating the correlations between runoff and the candidate input variables is presented in Figure 3. The analysis revealed that only the correlation coefficients for precipitation, temperature, and runoff exceeded 0.5. Consequently, the selected inputs were precipitation, temperature, and historical runoff. The lag times between current runoff and historical runoff, as well as between precipitation and temperature, were determined using a time lag cross-correlation method. Subsequently, the input and output samples were prepared for the batch-trained models. Eighty percent of the samples were allocated for training, while the remaining 20% were designated for testing.

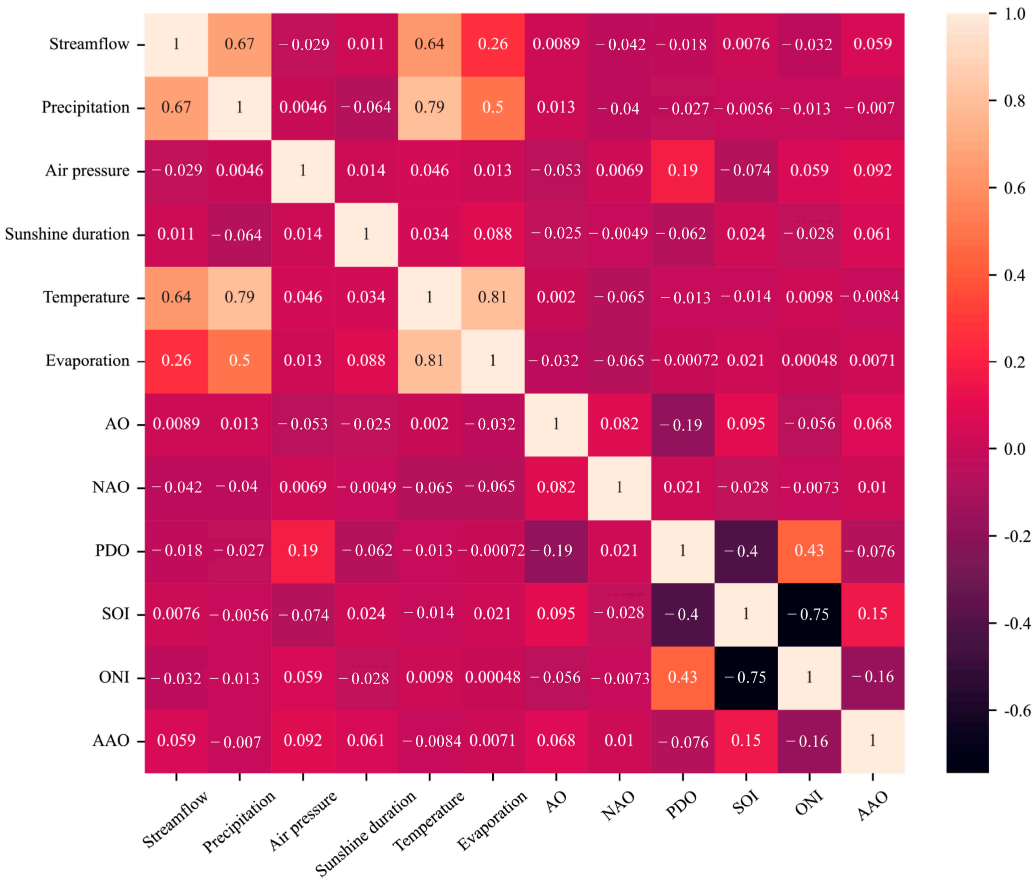

Figure 3. Heatmap of correlations between runoff and the candidate input variables.

The impact of various input combinations on the performance of the LSTM models was assessed. Four distinct input combinations were utilized: (a) all eleven candidate input variables; (b) only precipitation, temperature, and historical runoff; (c) precipitation, temperature, and historical runoff with corresponding lagged times; and (d) precipitation, temperature, and antecedent runoff, along with corresponding lagged times and static variables such as the Digital Elevation Model (DEM) and Normalized Difference Vegetation Index (NDVI), which provide essential information about the underlying surface. Figure 4 illustrates the performance of various input combinations using the KGE metric. As indicated in Table 1, the model produced KGE values of 0.46, 0.43, 0.64, and 0.80 for different input combinations. The proportions of grids with KGE values exceeding 0.6 were 95.29% for the LSTM model with input d and 25.13% for the LSTM model with input a. Additionally, the proportions of grids with KGE values surpassing 0.8 were 54.97% for the LSTM model with input d and 4.19% for the LSTM model with input c. Notably, there were no grids with KGE values exceeding 0.8 for the LSTM model using inputs a and b. These results demonstrate that incorporating additional information about static variables can enhance the accuracy of runoff projections.

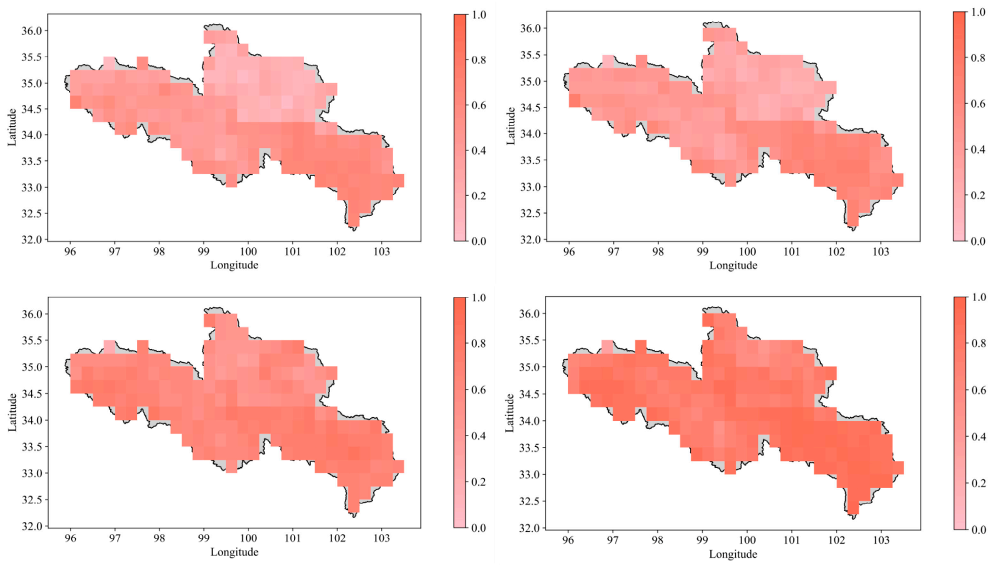

Figure 4. Performance of different input combinations (KGE). The KGE value is a comprehensive metric for evaluating model performance. The closer the value of KGE is to 1, the higher the accuracy of the LSTM model, representing a more accurate description and calculation of the relationship between precipitation, temperature, and historical runoff.

Table 1. Average values of KGE for the models with different input combinations.

		KGE	
	Average	**>0.6**	**>0.8**
Input a	0.46	25.13%	0
Input b	0.43	22.51%	0
Input c	0.64	69.11%	4.19%
Input d	0.80	95.29%	54.97%

4.2. LSTM Modelling

The output variables are defined as monthly runoff for a grid, and the input variables include static variables and dynamic variables. Dynamic variables were determined by eleven candidate input variables and their lagged time for each grid. Four different models were applied in the study area: multiple linear regression (MLR), the radial basis function neural network (RBFNN), the recurrent neural network (RNN), and long short-term memory (LSTM). The values of R^2, Kling–Gupta Efficiency (KGE), Nash–Sutcliffe Efficiency (NSE), and root-mean-square error (RMSE) were evaluated. Figures 5 and 6 illustrate the distributions of the four assessment metrics throughout the training and testing phases. Table 2 displays the average values of these metrics for the models during both training and testing. During the training phase, the R^2 values of the LSTM model increased by 60.00%, 17.33%, and 8.64% compared to the other three models, respectively. The KGE values also increased by 46.77%, 26.39%, and 5.81%. This indicates that, in terms of model correlation, bias, and variability, the LSTM model performed more comprehensively than the other three models. The NSE coefficient of the LSTM model was the highest at 0.90, outperforming the MLR and RNN models, although it fell slightly short of the RBFNN model. During the testing period, the LSTM model outperformed the MLR, RBFNN, and RNN models. Specifically, 94.24% of the grid R^2 values for the LSTM model exceeded 0.6, and both KGE values for the grid were above 0.6 in 95.29% of cases. Notably, the LSTM achieved the highest average R^2 value of 0.83 during testing, representing significant increases of 29.69%, 22.06%, and 6.41% over the other three models. Additionally, the LSTM model yielded the highest average KGE of 0.80, showing improvements of 45.45%, 33.33%, and 2.56%, respectively, compared to the alternative models. The LSTM model had an NSE value of 0.77, which was slightly lower than that of the RBFNN, but it achieved the lowest RMSE of 3.01. The comprehensive analysis of these metrics indicates that the LSTM model is well suited for runoff projection at a grid scale in the YRSR, offering superior predictive capabilities.

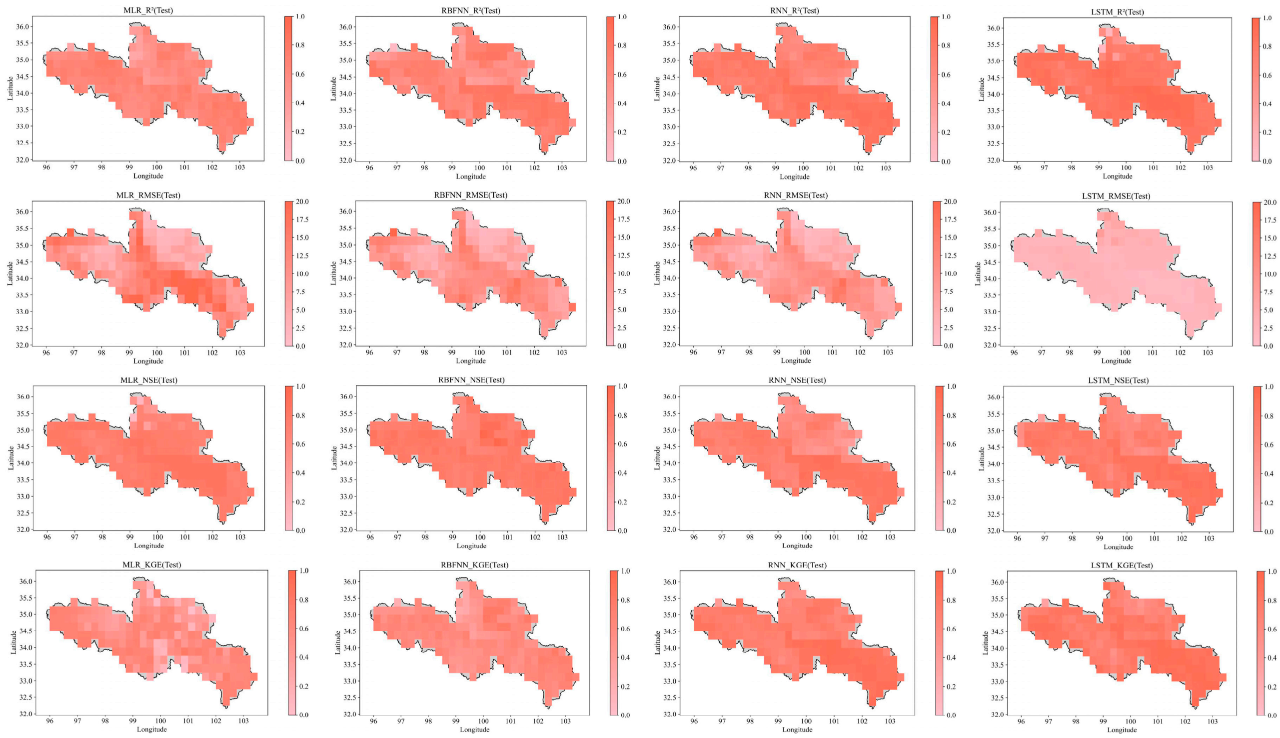

Figure 5. Spatial distribution maps of R^2, KGE, NSE, and RMSE during the training period.

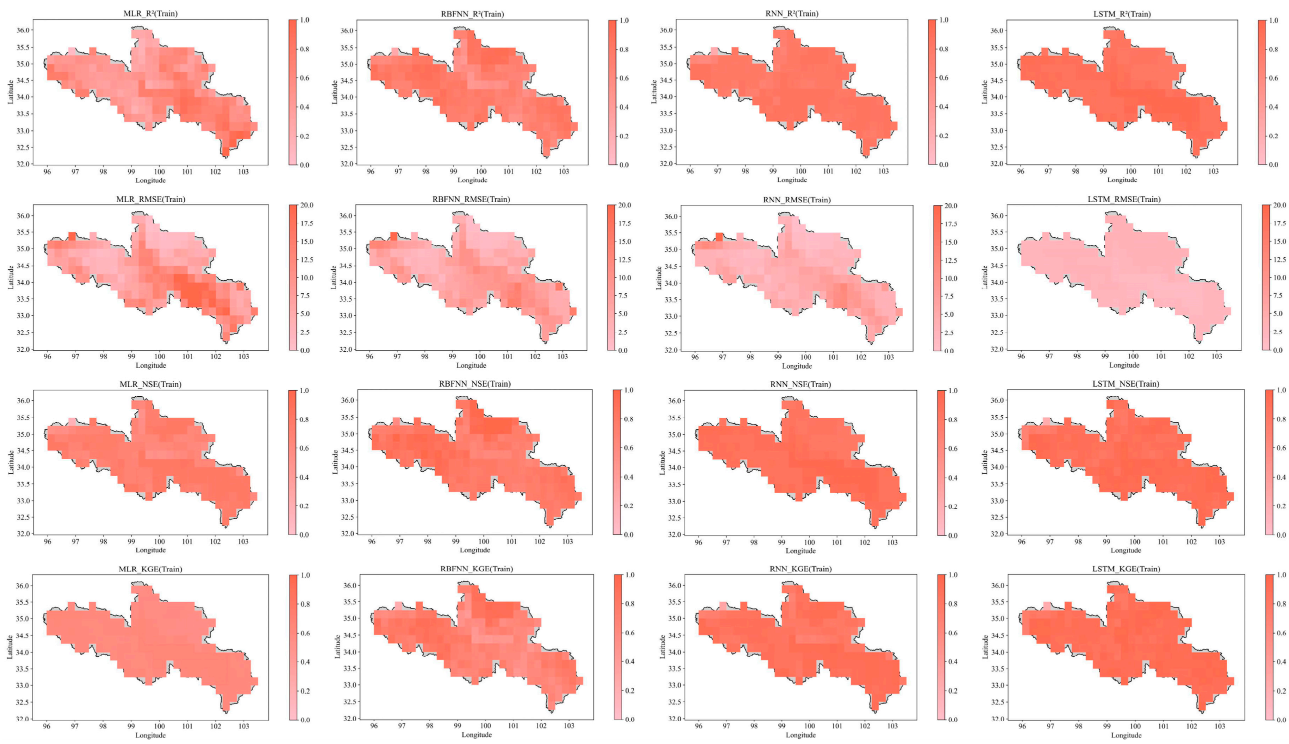

Figure 6. Spatial distribution maps of R^2, KGE, NSE, and RMSE during the testing period.

Table 2. Average values of the four evaluation metrics for the models of different periods.

		MLR	RBFNN	RNN	LSTM
training	R^2	0.55	0.75	0.81	0.88
	KGE	0.62	0.72	0.86	0.91
	NSE	0.72	0.81	0.88	0.90
	RMSE	8.94	6.77	4.80	2.63
testing	R^2	0.64	0.68	0.78	0.83
	KGE	0.55	0.60	0.78	0.80
	NSE	0.75	0.78	0.72	0.77
	RMSE	11.33	9.34	8.46	3.01

After developing the LSTM model, runoff projections can be generated as long as future precipitation and temperature data are provided as input to the well-trained LSTM models. The CanESM5 climate model will be employed to create future precipitation and temperature scenarios, including SSP126, SSP245, SSP370, and SSP585. SSP1-2.6 represents a Shared Socioeconomic Pathway characterized by the adoption of emission reduction policies and sustainable development strategies, while SSP5-8.5 signifies a future socioeconomic pathway with high emissions and extensive carbon use. According to the findings, runoff variability in the YRSR is expected to remain low and stable throughout the upcoming socioeconomic scenarios (2016–2045). For SSP1-2.6, SSP2-4.5, SSP3-7.0, and SSP5-8.5, the corresponding average annual runoff values are 204.68 mm, 201.85 mm, 229.0 mm, and 207.16 mm, respectively (Table 3). The estimated runoff values show minimal variation across the different scenarios. Notably, runoff under SSP5-8.5 demonstrates an increasing trend with the highest growth rate, followed by SSP3-7.0 and SSP2-4.5, while runoff under SSP1-2.6 exhibits a declining trend (Figure 7).

Table 3. Characteristics of monthly and annual runoff projections under the four SSPs.

	Monthly Runoff (mm)			Annual Runoff (mm)		
	Mean	Max	Min	Mean	Max	Min
SSP1-2.6	17.06	47.63	5.21	204.68	240.62	157.77
SSP2-4.5	16.82	43.51	5.13	201.85	240.91	166.35
SSP3-7.0	16.82	43.38	5.23	229.00	299.88	188.81
SSP5-8.5	17.26	48.33	5.22	207.16	246.36	157.19

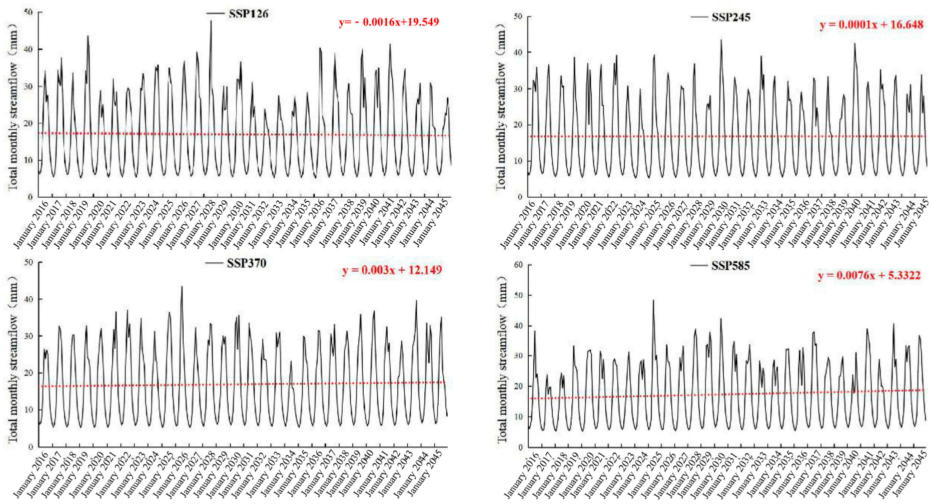

Figure 7. Time series of future runoff projections from YRSR under different SSPs (2016–2045).

Runoff under the SSP5-8.5 scenario exhibits the most significant fluctuations in peak values, with a 95% confidence interval ranging from 157.19 to 246.36 mm for the annual average runoff. This indicates that extreme precipitation events may increase in the future, especially in summer. Therefore, it is necessary to strengthen the flood warning system in the source area of the Yellow River and to formulate flood prevention measures in advance to reduce the impact of floods on downstream areas. The overall trend remains relatively stable, with SSP2-4.5 demonstrating the fastest growth among the four scenarios, followed by SSP3-7.0 and SSP5-8.5. In contrast, SSP1-2.6 continues to show a decreasing trend, with a more pronounced decline compared to the 2016–2045 period. This indicates the need to strengthen drought monitoring and water resource allocation, especially during periods of high demand for agricultural irrigation and ecological water use. Additionally, the spatial distribution of runoff gradually increases from the northwest to the southeast, with the lowest runoff levels recorded in Northeast China, followed by Southwest China, providing a basis for the dynamic management of ecological flow. Figure 8 illustrates the average runoff distribution for the next 30 years in the YRSR. The average discharge progressively rises from the northwest to the southeast, with the lowest flow observed in the northeast and the second lowest in the southwest. The results highlight the profound impact of climate change on the water resources in the source region of the Yellow River. In the future, efforts should be made to strengthen the construction of climate change adaptation capabilities, such as optimizing reservoir scheduling, promoting water-saving technologies, and enhancing comprehensive watershed management to achieve the sustainable use of water resources. Runoff predictions under different SSP scenarios are different and are mainly influenced by climate change, socioeconomic development, and ecological response. These differences provide an important scientific basis for water resource management in the source region of the Yellow River. Under more extreme climate change conditions, the hydrological processes of the basin may change.

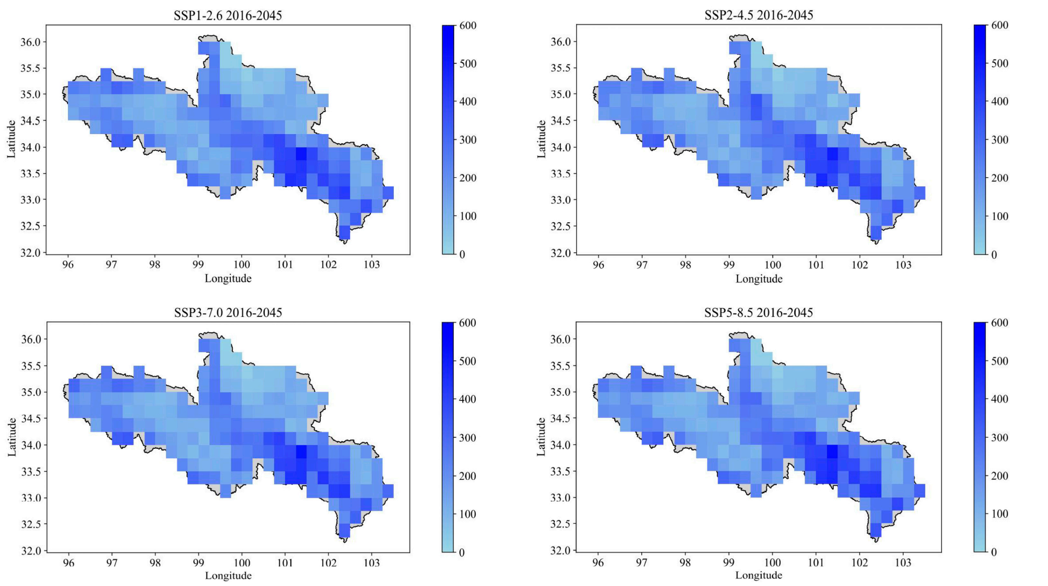

Figure 8. Distribution of future runoff projections in the YRSR under different SSPs.

4.3. Uncertainty

The confidence intervals for runoff predictions were evaluated while accounting for uncertainty in the parameters of the LSTM model. Figures 9 and 10 illustrate the confidence intervals for monthly runoff from 2016 to 2045, as well as the runoff forecast for January 2030, which represents the probable distribution of runoff projections during that period. According to four Shared Socioeconomic Pathways (SSPs), the monthly runoff in January

2030 is expected to range primarily between 4.0 and 5.2 mm, 8.0 and 10.0 mm, 10.0 and 12.0 mm, and 9.0 and 11.0 mm. The 95% confidence interval for monthly runoff across all grids in the study area, as covered by SSP5-8.5, is estimated to be between 12.37 mm and 24.68 mm.

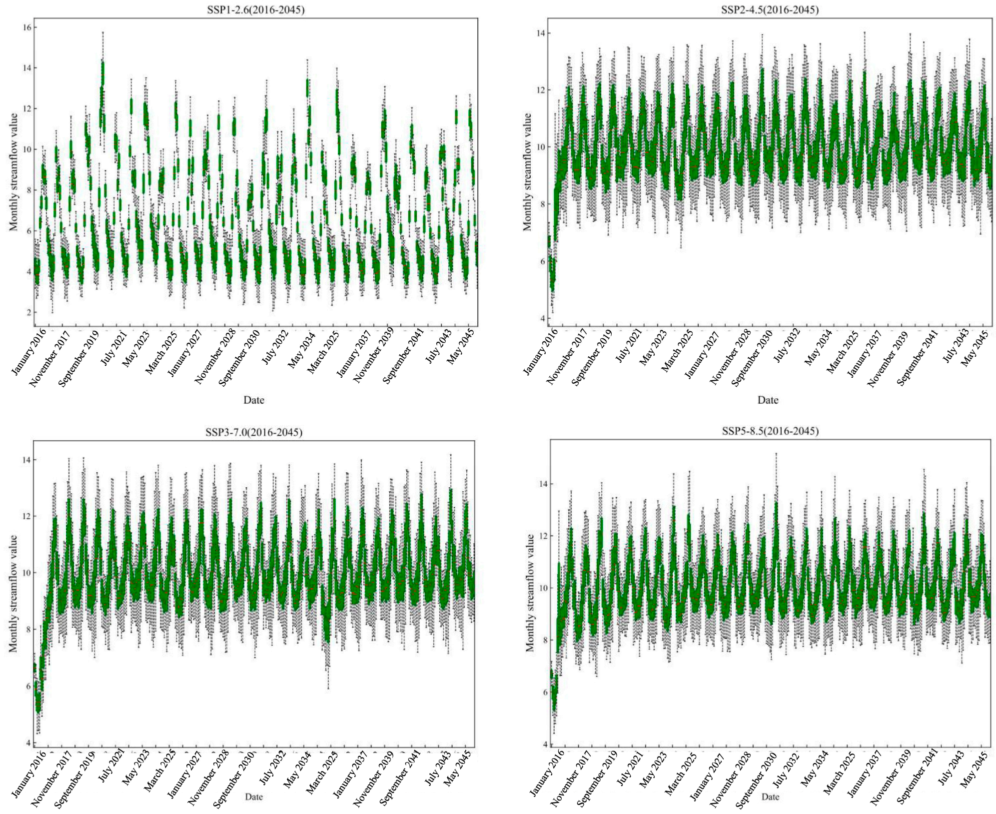

Figure 9. Boxplot of confidence intervals for monthly runoff from 2016 to 2045 for a grid.

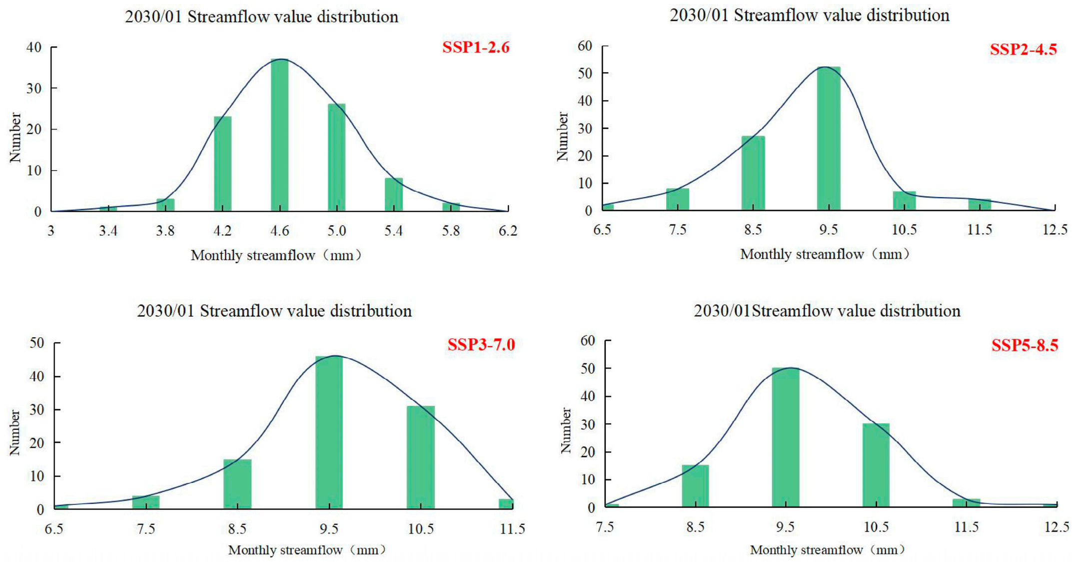

Figure 10. Distribution of runoff values at January 2030.

Limited research has been conducted on runoff estimates considering climate change in the YRSR. Lu et al. (2018) reported that streamflow is projected to increase by more than 3% in the YRSR during the future period of 2041–2060, based on a regional climate model (RegCM4) and the Variable Infiltration Capacity (VIC) model. Under the representative concentration pathways (RCPs), the mean runoff projections were 8565.32 m^3/s, 8823.59 m^3/s, and 8074.54 m^3/s for the three RCPs [31]. Ma et al. (2021) found that runoff in the YRSR is expected to accelerate by 0.42 m^3/s per year from 2020 to 2040, as determined by the Elman neural network model [32].

These findings align with the forecasts made by Li et al. (2022) for the period from 2021 to 2060 [33]. Zhou et al. (2023) employed six CMIP6 General Circulation Models (GCMs) along with the Variable Infiltration Capacity (VIC) hydrological model to predict a 10–20% increase in annual runoff depth in the Yellow River basin between 2020 and 2049 [15]. The expected runoff under CMIP6 is projected to be greater than that under CMIP5, as the anticipated future precipitation under CMIP6 exceeds that of CMIP5 [34,35].

Based on the current literature, there is limited research on the application of CMIP6 data for future runoff predictions in the source region [36–38]. Most studies have primarily focused on utilizing CMIP5 data. Additionally, various studies have employed different climate models, each emphasizing distinct data production processes, which can lead to significant variations in the results generated by the same model. Moreover, discrepancies may exist in the duration of future projections and the comprehensive calculation of characteristic values or trends. Overall, the length of future predictions, the choice between climate models (CMIP5 or CMIP6), and the selection of projection models, such as SWAT, VIC, or deep learning models, influence the trends and quantities of runoff predictions. According to several assessments, the projected runoff pattern in the YRSR has either slightly increased or remained unchanged. This finding aligns with our conclusions. Water resource management holds significant importance in practical applications such as flood warning and drought monitoring. The high accuracy of the LSTM model makes runoff forecasting more reliable for practical applications in the source area of the Yellow River.

5. Conclusions

Using input selection, LSTM modelling, and Monte Carlo simulations under future climate scenarios, a grid-based LSTM runoff projection and uncertainty framework was employed to forecast future changes in runoff in the YRSR (e.g., SSP1-2.6, SSP2-4.5, SSP3-7.0, and SSP5-8.5). The results of input selection indicated that precipitation and temperature were identified as significant variables. Static variables, including the Digital Elevation Model (DEM) and Normalized Difference Vegetation Index (NDVI), were utilized as input variables to provide additional information, enhancing the accuracy of runoff projections from 0.46 to 0.80. LSTM models demonstrated the capability to accurately represent the relationships among precipitation, temperature, historical runoff, and future runoff at the grid scale. The LSTM model achieved the highest mean Kling–Gupta Efficiency (KGE) score of 0.80, reflecting improvements of 45.45%, 33.33%, and 2.56%, respectively, over the other three models. Multiple metrics indicate that LSTM models are particularly effective for runoff projection in the YRSR, showcasing enhanced predictive capabilities. The projected runoff in the YRSR is anticipated to experience a moderate increase from 2016 to 2045, with average annual runoff gradually increasing from northwest to southeast. Considering the uncertainty associated with LSTM parameters, annual runoff is expected to rise, with projection ranges of 148.44–296.16 mm at the 95% confidence level across various climate scenarios. This methodology is essential for the efficient management of water resources and the promotion of sustainable economic development within the YRSR region, especially in light of potential ongoing increases in surface temperatures. In this paper, we did not explore LSTM models guided by physical mechanisms to enhance performance, indicating a need for further investigation into this topic. Additionally, further discussion is warranted regarding the details of this framework, including the incorporation of additional machine learning techniques, addressing model scalability, and testing the framework under different climate scenarios.

Author Contributions: H.C.: Methodology, data preparation, validation, writing, supervision, summary conclusion. Y.J.: Methodology, data collection, data preprocessing, code, visualization, writing. Z.W.: Methodology, data collection, code, formal analysis, visualization, writing. All authors have read and agreed to the published version of the manuscript.

Funding: The authors declare that this study received funding from the Major Science and Technology Projects of Qinghai Province (2021-SF-A6) and the National Natural Science Foundation (42207070). The funder was not involved in the study design, collection, analysis, interpretation of data, the writing of this article or the decision to submit it for publication.

Data Availability Statement: Data may be provided upon request due to privacy or ethical restrictions. The data presented in this study are available on request from the corresponding authors. This data is not publicly available due to privacy concerns.

Acknowledgments: This work was sponsored in part by the Major Science and Technology Projects of Qinghai Province (2021-SF-A6) and the National Natural Science Foundation (42207070). The author would like to thank the reviewers and editors for their valuable comments and suggestions.

Conflicts of Interest: Author Zhuoqi Wang was employed by the company Beijing Goldenwater Information Technology Co., Ltd. The remaining authors declare that the research was conducted in the absence of any commercial or financial relationships that could be construed as a potential conflict of interest.

References

1. Huang, Y.; Xiao, W.; Hou, B.; Zhou, Y.; Hou, G.; Yi, L.; Cui, H. Hydrological projections in the upper reaches of the Yangtze River Basin from 2020 to 2050. *Sci. Rep.* **2021**, *11*, 9720. [CrossRef] [PubMed]
2. Mo, R.; Xu, B.; Zhong, P.-A.; Dong, Y.; Wang, H.; Yue, H.; Zhu, J.; Wang, H.; Wang, G.; Zhang, J. Long-term probabilistic streamflow forecast model with "inputs–structure–parameters" hierarchical optimization framework. *J. Hydrol.* **2023**, *622*, 129736. [CrossRef]
3. Belvederesi, C.; Zaghloul, M.S.; Achari, G.; Gupta, A.; Hassan, Q.K. Modelling river flow in cold and ungauged regions: A review of the purposes, methods, and challenges. *Environ. Rev.* **2022**, *30*, 159–173. [CrossRef]
4. Tursun, A.; Xie, X.; Wang, Y.; Liu, Y.; Peng, D.; Zheng, B. Enhancing streamflow simulation in large and human-regulated basins: Long short-term memory with multiscale attributes. *J. Hydrol.* **2024**, *630*, 130771. [CrossRef]
5. Sahoo, B.B.; Jha, R.; Singh, A.; Kumar, D. Long short-term memory (LSTM) recurrent neural network for low-flow hydrological time series forecasting. *Acta Geophys.* **2019**, *67*, 1471–1481. [CrossRef]
6. Xiang, Z.; Yan, J.; Demir, I. A rainfall-runoff model with LSTM-based sequence-to-sequence learning. *Water Resour. Res.* **2020**, *56*, e2019WR025326. [CrossRef]
7. Hunt, K.M.R.; Matthews, G.R.; Pappenberger, F.; Prudhomme, C. Using a long short-term memory (LSTM) neural network to boost river streamflow forecasts over the western United States. *Hydrol. Earth Syst. Sci.* **2022**, *26*, 5449–5472. [CrossRef]
8. Khoshkalam, Y.; Rousseau, A.N.; Rahmani, F.; Shen, C.; Abbasnezhadi, K. Applying transfer learning techniques to enhance the accuracy of streamflow prediction produced by long Short-term memory networks with data integration. *J. Hydrol.* **2023**, *622*, 129682. [CrossRef]
9. Xu, L.; Chen, N.; Chen, Z.; Zhang, C.; Yu, H. Spatiotemporal forecasting in earth system science: Methods, uncertainties, predictability and future directions. *Earth-Sci. Rev.* **2021**, *222*, 103828. [CrossRef]
10. Usman, M.; Ndehedehe, C.E.; Farah, H.; Manzanas, R. Impacts of Climate Change on The Streamflow of A Large River Basin in the Australian Tropics Using Optimally Selected Climate Model Outputs. *J. Clean. Prod.* **2021**, *315*, 128091. [CrossRef]
11. Zhang, L.; Yuan, F.; Wang, B.; Ren, L.; Zhao, C.; Shi, J.; Liu, Y.; Jiang, S.; Yang, X.; Chen, T.; et al. Quantifying uncertainty sources in extreme flow projections for three watersheds with different climate features in China. *Atmos. Res.* **2021**, *249*, 105331. [CrossRef]
12. Ejaz, F.; Guthke, A.; Wöhling, T.; Nowak, W. Comprehensive uncertainty analysis for surface water and groundwater projections under climate change based on a lumped geo-hydrological model. *J. Hydrol.* **2023**, *626*, 130323. [CrossRef]
13. Liu, L.; Liu, Z.; Ren, X.; Fischer, T.; Xu, Y. Hydrological impacts of climate change in the Yellow River Basin for the 21st century using hydrological model and statistical downscaling model. *Quat. Int.* **2011**, *244*, 211–220. [CrossRef]
14. Ji, P.; Yuan, X.; Jiao, Y. Future hydrological drought changes over the upper Yellow River basin: The role of climate change, land cover change and reservoir operation. *J. Hydrol.* **2023**, *617*, 129128. [CrossRef]
15. Zhou, J.; Lu, H.; Yang, K.; Jiang, R.; Yang, Y.; Wang, W.; Zhang, X. Projection of China's future runoff based on the CMIP6 mid-high warming scenarios. *Sci. China Earth Sci.* **2023**, *66*, 528–546. [CrossRef]

16. Cheng, M.; Fang, F.; Kinouchi, T.; Navon, I.; Pain, C. Long lead-time daily and monthly streamflow forecasting using machine learning methods. *J. Hydrol.* **2020**, *590*, 125376. [CrossRef]
17. Tikhamarine, Y.; Souag-Gamane, D.; Ahmed, A.N.; Kisi, O.; El-Shafie, A. Improving artificial intelligence models accuracy for monthly streamflow forecasting using grey Wolf optimization (GWO) algorithm. *J. Hydrol.* **2020**, *582*, 124435. [CrossRef]
18. Gauch, M.; Kratzert, F.; Klotz, D.; Nearing, G.; Lin, J.; Hochreiter, S. Rainfall–runoff prediction at multiple timescales with a single Long Short-Term Memory network. *Hydrol. Earth Syst. Sci.* **2021**, *25*, 2045–2062. [CrossRef]
19. Hashemi, R.; Brigode, P.; Garambois, P.-A.; Javelle, P. How can we benefit from regime information to make more effective use of long short-term memory (LSTM) runoff models? *Hydrol. Earth Syst. Sci.* **2022**, *26*, 5793–5816. [CrossRef]
20. Feng, D.; Fang, K.; Shen, C. Enhancing streamflow forecast and extracting insights using long-short term memory networks with data integration at continental scales. *Water Resour. Res.* **2020**, *56*, e2019WR026793. [CrossRef]
21. Lees, T.; Buechel, M.; Anderson, B.; Slater, L.; Reece, S.; Coxon, G.; Dadson, S.J. Benchmarking data-driven rainfall–runoff models in Great Britain: A comparison of long short-term memory (LSTM)-based models with four lumped conceptual models. *Hydrol. Earth Syst. Sci.* **2021**, *25*, 5517–5534. [CrossRef]
22. Dehghani, M.; Saghafian, B.; Saleh, F.N.; Farokhnia, A.; Noori, R. Uncertainty analysis of streamflow drought forecast using artificial neural networks and Monte-Carlo simulation. *Int. J. Clim.* **2014**, *34*, 1169–1180. [CrossRef]
23. Alipour, S.M.; Engeland, K.; Leal, J. Uncertainty analysis of 100-year flood maps under climate change scenarios. *J. Hydrol.* **2024**, *628*, 130502. [CrossRef]
24. Su, F.; Zhang, L.; Ou, T.; Chen, D.; Yao, T.; Tong, K.; Qi, Y. Hydrological response to future climate changes for the major upstream river basins in the Tibetan Plateau. *Glob. Planet. Change* **2016**, *136*, 82–95. [CrossRef]
25. Hu, J.; Wu, Y.; Sun, P.; Zhao, F.; Sun, K.; Li, T.; Sivakumar, B.; Qiu, L.; Sun, Y.; Jin, Z. Predicting long-term hydrological change caused by climate shifting in the 21st century in the headwater area of the Yellow River Basin. *Stoch. Environ. Res. Risk Assess.* **2021**, *36*, 1651–1668. [CrossRef]
26. Hu, F.; Yang, Q.; Yang, J.; Luo, Z.; Shao, J.; Wang, G. Incorporating multiple grid-based data in CNN-LSTM hybrid model for daily runoff prediction in the source region of the Yellow River Basin. *J. Hydrol. Reg. Stud.* **2024**, *51*, 101652. [CrossRef]
27. Gou, J.; Miao, C.; Samaniego, L.; Xiao, M.; Wu, J.; Guo, X. CNRD v1.0: A high-quality natural runoff dataset for hydrological and climate studies in China. *Bull. Am. Meteorol. Soc.* **2021**, *102*, E929–E947. [CrossRef]
28. Singh, D.; Vardhan, M.; Sahu, R.; Chatterjee, D.; Chauhan, P.; Liu, S. Machine-learning- and deep-learning-based streamflow prediction in a hilly catchment for future scenarios using CMIP6 GCM data. *Hydrol. Earth Syst. Sci.* **2023**, *27*, 1047–1075. [CrossRef]
29. Mohseni, U.; Agnihotri, P.G.; Pande, C.B.; Durin, B. Understanding the climate change and land use impact on streamflow in the present and future under CMIP6 climate scenarios for the Parvara Mula Basin, India. *Water* **2023**, *15*, 1753. [CrossRef]
30. Xiao, H.; Zhuo, Y.; Jiang, P.; Zhao, Y.; Pang, K.; Zhang, X. Evaluation and projection of extreme precipitation using CMIP6 model simulations in the Yellow River Basin. *J. Water Clim. Change* **2024**, *15*, 2326–2347. [CrossRef]
31. Lu, W.; Wang, W.; Shao, Q.; Yu, Z.; Hao, Z.; Xing, W.; Yong, B.; Li, J. Hydrological projections of future climate change over the source region of Yellow River and Yangtze River in the Tibetan Plateau: A comprehensive assessment by coupling RegCM4 and VIC model. *Hydrol. Process.* **2018**, *32*, 2096–2117. [CrossRef]
32. Ma, Q.; Dai, C.; Jin, H.; Liang, S.; Bense, V.F.; Lan, Y.; Marchenko, S.S.; Wang, C. Streamflow changes in the headwater area of yellow river, ne Qinghai-Tibet plateau during 1955–2040 and their implications. *Water* **2021**, *13*, 1360. [CrossRef]
33. Li, X.; Jia, H.; Chen, Y.; Wen, J. Runoff simulation and projection in the source area of the Yellow River using the SWAT model and SSPs scenarios. *Front. Environ. Sci.* **2022**, *10*, 1012838. [CrossRef]
34. Zhu, X.; Lee, S.-Y.; Wen, X.; Ji, Z.; Lin, L.; Wei, Z.; Zheng, Z.; Xu, D.; Dong, W. Extreme climate changes over three major river basins in China as seen in CMIP5 and CMIP6. *Clim. Dyn.* **2021**, *57*, 1187–1205. [CrossRef]
35. Guo, Y.; Yu, X.; Xu, Y.-P.; Wang, G.; Xie, J.; Gu, H. A comparative assessment of CMIP5 and CMIP6 in hydrological responses of the Yellow River Basin, China. *Hydrol. Res.* **2022**, *53*, 867–891. [CrossRef]
36. Sedighkia, M.; Datta, B. Using evolutionary algorithms for continuous simulation of long-term reservoir inflows. *Proc. Inst. Civ. Eng.-Water Manag.* **2022**, *175*, 67–77. [CrossRef]
37. Man, Y.; Yang, Q.; Shao, J.; Wang, G.; Bai, L.; Xue, Y. Enhanced LSTM model for daily runoff prediction in the upper Huai river basin, China. *Engineering* **2023**, *24*, 229–238. [CrossRef]
38. Xu, Y.; Hu, C.; Wu, Q.; Jian, S.; Li, Z.; Chen, Y.; Zhang, G.; Zhang, Z.; Wang, S. Research on particle swarm optimization in LSTM neural networks for rainfall-runoff simulation. *J. Hydrol.* **2022**, *608*, 127553. [CrossRef]